Study by EELS of helium bubbles in a martensitic steel

S. Fréchard [a], M. Walls [b,*], M. Kociak [b], J.P. Chevalier [c], J. Henry [d], D. Gorse [a]

[a] *Institut de Chimie et des Matériaux Paris-Est, 15, rue Georges Urbain, 94407 Vitry-sur-Seine, France*
[b] *Laboratoire de Physique des Solides UMR 8502, Université Paris-Sud, 91405 Orsay cedex, France*
[c] *Conservatoire National des Arts et Métiers, 292, rue Saint-Martin, 75141 Paris cedex, France*
[d] *CEA, DEN, SRMA, F-91191 Gif-sur-Yvette, France*

ARTICLE INFO

ABSTRACT

This work presents measurements of the helium density and pressure in small bubbles in a martensitic steel, which is a vital first step towards identifying their role in the microstructural mechanisms determining the macroscopic properties of the material. Electron Energy-Loss Spectroscopy in the Scanning Transmission Electron Microscope has been used to analyse individual bubbles. The energy shift of the $1s \rightarrow 2p$ transition and the helium density have been measured for each bubble analysed. The pressure inside the bubbles has been calculated from the helium density using an equation of state. In these bubbles, the values for the helium pressure seem to be smaller than the equilibrium pressure, and agree in trend with the findings of previous studies, although our results extend to smaller radii and higher pressures.

1. Introduction

This paper presents a study of homogeneously α-implanted specimens of a 9Cr–1Mo (EM10) martensitic steel at 550 °C to a concentration of 5000 appm. At this implantation temperature, He bubbles are easily observed by conventional TEM. The bubble number density and size had been previously determined [3,4]. However the He density itself is not attainable by conventional TEM. This is the motivation for the study of He bubbles by Electron Energy-Loss Spectroscopy (EELS).

Such bubbles can be produced under certain irradiation conditions in metallic materials due to the extremely low He solubility. The bubbles can cause a significant loss of ductility. This subject is of concern for the steels to be used in the future for fusion applications; embrittlement by helium is regarded as one of the effects which could limit the lifetime of structural materials in this context. Many investigations have already been conducted to identify the effect of He bubbles on metal mechanical properties. The initial studies [5–7] aimed at understanding the mechanism of He bubble formation. The influence of implantation conditions on bubble size distributions [8] and the effect of implanted He on the mechanical properties [9] have been studied and it has been shown that helium can induce a severe loss of ductility [3,4]. Thus, it is important to understand the mechanisms involved in formation and growth of the bubbles.

Knowledge of the He density existing in these small bubbles is prerequisite for this. Recent experimental studies [2,10] have shown that Scanning Transmission Electron Microscopy combined with Electron Energy-Loss Spectroscopy (STEM–EELS) is a powerful technique for He bubble analysis. It can be used to calculate the He density in individual bubbles.

The aim of this work is to obtain the helium density and pressure in very small bubbles. The He density is directly measured from the electron energy-loss signal, using a method developed by Walsh et al. [2]. Then, the appropriate equation of state [1] can be used to calculate the pressure in the bubbles from the He density.

2. Experimental procedure

2.1. Microstructural observations

He bubbles were first examined by Transmission Electron Microscopy (TEM). Following implantation and testing of tensile specimens, a 2 mm diameter disc was punched from the gauge section of each specimen and thin foils suitable for TEM examinations were prepared by jet-electropolishing. A JEOL 2000 EX and a TEM TECNAI F20 were used for standard observations (images and diffraction). In order to observe the He bubbles, a negative defocus was used, generating Fresnel fringe contrast around the bubbles. Energy-loss analyses were performed in a VG HB501 STEM operat-

ing at 100 kV, and equipped with a GATAN 666 spectrometer. Details of this technique are presented in Section 3.

2.2. Material

The material investigated in this study is a martensitic steel (EM10 grade). The nominal chemical composition is given in Table 1.

Plates with an initial thickness of 0.5 mm were cold-rolled to a final thickness of about 100 μm. After rolling, heat treatments were carried out. The following normalisation and tempering conditions were applied: 1 h at 1050 °C plus 1 h at 760 °C. The resulting microstructure of the steel consisted of 200-300 nm wide martensite laths in the prior-austenite grains of average size 21 μm. The specimens were implanted with 5000 appm He at 550 °C. The irradiation apparatus is located at a beam line of the Jülich Compact Cyclotron. The initial energy of the α-beam (27.4 MeV) was then degraded by a rotating wheel consisting of 24 aluminium foils of different thicknesses. In order to obtain a homogeneous implantation, the beam was scanned at sawtooth frequencies of typically 300 Hz in both directions across the specimen. More details of the He implantation process are given by Henry et al. [4]. Before TEM characterisation, the implanted specimens were mechanically tested at room temperature. The results of these tensile tests are presented in Ref. [4]. Tensile tests performed on EM10 samples implanted to 0.5 at.% He at 550 °C indicated helium-induced hardening. However, significant ductility was retained at this implantation temperature. After He implantation and mechanical characterisation, the microstructure (Fig. 1) shows He bubbles nucleated at dislocations, lath and sub-boundaries and precipitates.

The bubbles are small (average diameter 5–10 nm) and clearly facetted (Fig. 2). Fig. 2(a) and (b) shows TEM images along ⟨1 1 1⟩ and ⟨1 1 3⟩ directions respectively. The bubbles appear for the most part as hexagons in the ⟨1 1 1⟩ direction (Fig. 2(a)) and as somewhat irregular rectangles or parallelograms in the ⟨1 1 3⟩ direction (Fig. 2(b)). The bubbles are thus most likely to be cuboids in which the facets are parallel to the (1 0 0) planes. This feature is

Table 1
Chemical composition of EM10 (in wt%).

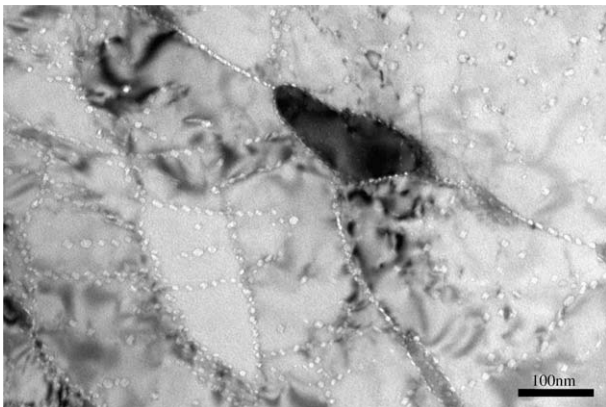| Steel	C	Cr	Mo	V	Nb	Ni	Mn	N	P	Si
EM10	0.1	8.8	1.09	–	–	0.18	0.51	0.02	0.02	0.37

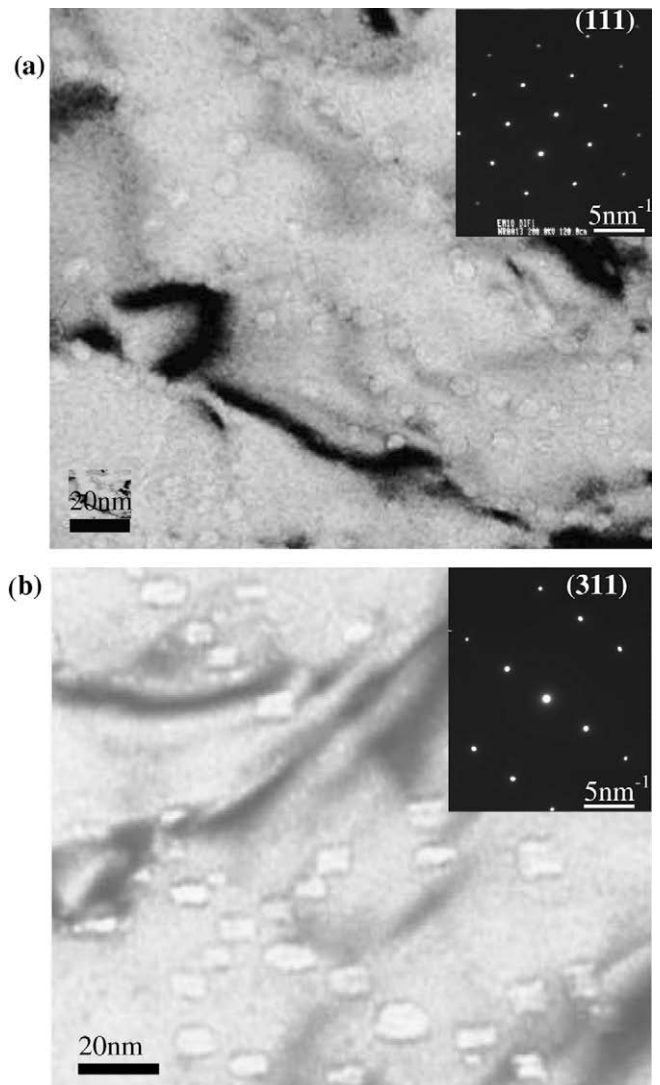**Fig. 1.** TEM micrograph of typical He bubble microstructure in EM10 post implantation.

Fig. 2. (a) TEM bright field micrograph obtained along the [1 1 1] zone axis and the corresponding diffraction pattern and (b) TEM bf micrograph obtained along the [3 1 1] zone axis and the corresponding diffraction pattern.

consistent with the results of the literature [11,12]. In bcc metals, the {1 0 0} surface energy is significantly reduced compared with other orientations. Some bubbles are elongated. This elongation is not due to the stress created during the tensile tests; such microstructure has also been observed in unstressed implanted specimens.

3. Method of analysis

EELS experiments have been used before to measure the He density in bubbles [13–16]. The main result of these studies was that the energy of the 1s–2p transition, which is at 21.218 eV [18] for the dilute gas (or for the He free atom) is shifted towards higher energy in the bubbles. The peak position has also been measured by ultraviolet absorption. A linear relationship between the energy shift (ΔE) and the He density n is obtained:

$$\Delta E = Cn. \tag{1}$$

The energy shift can thus be used to determine the He density by calculating the proportionality coefficient C. Lucas [14] obtained

an estimation of C through calculations of the potential energy curves of the He₂ excimer. Taylor [16] used a multi-configurational self-consistent field to calculate the ground and excited state of a He atom surrounded by 12 other He atoms. The major disadvantage of the experiments described in [13–16] was that the electron beam size of the TEM used did not permit the analysis of individual bubbles, but rather sampled many bubbles of different sizes. A further problem, for the theoretical approaches is the complexity of the calculation for C.

Walsh et al. [1] therefore proposed a procedure for directly measuring the density of He atoms in individual bubbles of nanometre size using EELS in the STEM mode. The following equation gives the number density of He atoms in a bubble:

$$n_{He} = I_p/(\sigma_p I_z d). \tag{2}$$

I_z and I_p are respectively the intensities of the elastic peak and of the He $1s \rightarrow 2p$ peak. These intensities can be obtained from the EEL spectrum recorded in the centre of the bubble. d corresponds to the bubble thickness crossed by the electron beam. σ_p is the angle-integrated cross-section for the $1s \rightarrow 2p$ interaction evaluated for the experimental collection angles. Eq. (2) is valid, irrespective of the sample thickness up to a reasonable limit (of the order of several tens of nanometers) and of the position of the bubble in the foil thickness. The diameter of the electron beam should be smaller than the bubble diameter in order to obtain localised information on an individual bubble. Two major difficulties of the method are the measurement of the bubble diameter and the extraction of the $1s \rightarrow 2p$ peak from the experimental spectrum.

In this work, we follow the procedure initiated by Taverna et al. [10], which uses the spectrum-image (SPIM) mode to obtain better information on He bubbles. In this mode, both the HAADF and EELS signal are acquired in parallel as the probe scans the area of interest. By combining a very high spatial resolution with full spectroscopic information, this technique allows us to follow variations in the position and intensity of the $1s \rightarrow 2p$ energy at the same time and thus directly to correlate them with structural information on the bubble. More specifically, we used a "chronospim" approach, in which in order to increase the signal dynamics and signal-to-noise ratio, a large number of spectra are acquired at the same probe position, and are subsequently realigned and summed [17]. In this mode, the probe is scanned over the sample (in two directions) and for each pixel a complete energy-loss spectrum is recorded in the selected energy domain. In this work, SPIMs composed of 128×128 spectra were acquired under the following conditions: acquisition time 10 ms per spectrum, 50 spectra per pixel, probe size 0.7 nm with pixel sizes (i.e. probe steps) of around 0.5 nm, giving enough sampling in smaller bubbles of 2 nm radius. The energy dispersion was typically 0.05 eV per channel.

3.1. Extraction of the $1s \rightarrow 2p$ peak intensity

It is difficult to extract the He signal from the experimental spectrum. In our case, the peak due to the He 1s–2p transition is located near the plasmon maximum of the metallic matrix (Fig. 3(a)). Fig. 3(a) shows the EEL spectrum acquired from the centre of a He bubble. The He $1s \rightarrow 2p$ peak is found at 23 eV. The plasmon peak of iron has been fitted with a Gaussian curve presented in blue in Fig. 3(a). Fig. 3(b) shows the He signal obtained by subtracting the Gaussian curve from the experimental spectrum. The He signal is also modelled using a Gaussian. The intensity of the K-edge corresponds to the area under the Gaussian for an energy window of about 4 eV (21–25 eV). The $1s \rightarrow 2p$ energy is given by the position of the Gaussian maximum.
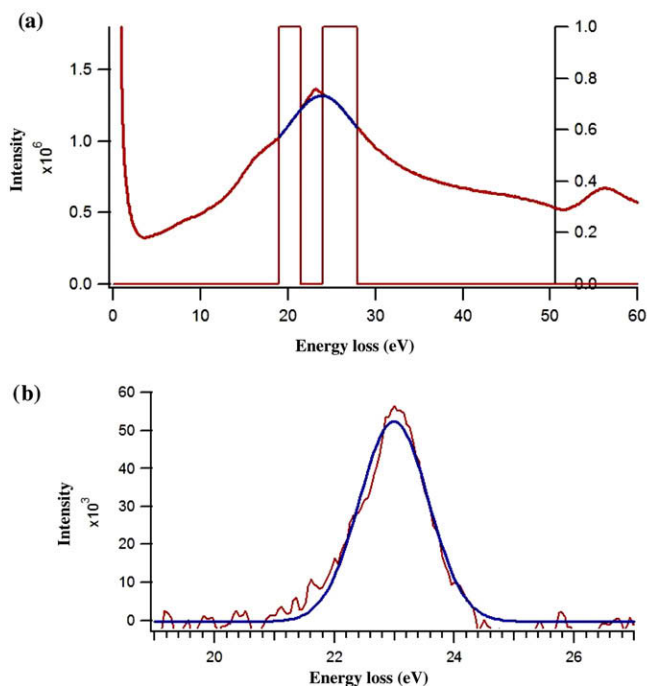

Fig. 3. (a) EEL spectrum recorded from the centre of a He bubble in the EM10 martensitic steel and (b) subtracted He signal and corresponding Gaussian fit: red: raw data blue: Plasmon fitting using the windows marked in red in part (a). (For interpretation of the references in colour in this figure legend, the reader is referred to the web version of this article.)

3.2. Measurement of the bubble diameter

Elongated bubbles were not analysed because of the difficulty of determining the He thickness crossed by the electron beam. Only bubbles with a regular shape have been studied. The He bubble thickness can thus be considered as the bubble diameter when the electron beam passes through the centre of the bubble. The bubble diameter is measured from the High Angle Annular Dark Field (HAADF) image by drawing intensity profiles. (This was deemed more accurate than using the bright field image, in which, at under-focus, the fresnel fringe contrast makes the edge of the bubble hard to define, and at focus the contrast is almost zero). Direct measurement of the bubble diameter can be subjective and depends on the contrast level. As already mentioned, the bubbles are not perfectly round. Several profiles were taken, crossing the bubble in different directions, and an average diameter was obtained. The value of the bubble thickness is thus likely to be a major source of error, both random and systematic.

4. Results

4.1. Bubbles and voids

TEM images of the sample show He bubbles having a typical radius between 2 and 6 nm. Fig. 4(a) is a HAADF (High Angle Annular Dark Field) image of the bubbles. For this work, several areas have been selected and studied by the spectrum-image technique. In Fig. 4(a), four bubbles can be seen. Fig. 4(b) shows the extracted He signal obtained from the bubbles in Fig. 4(a). One of theses exhibits no He signal (Fig. 4(b)). In fact, not all bubbles contain He atoms. Voids are present in the thin foils used for microscopy. For all the studied areas and all thicknesses of the thin foil, the proportion of empty voids is always in agreement with the probability that bubbles cut the surfaces of the thin foil. A simple interpreta-
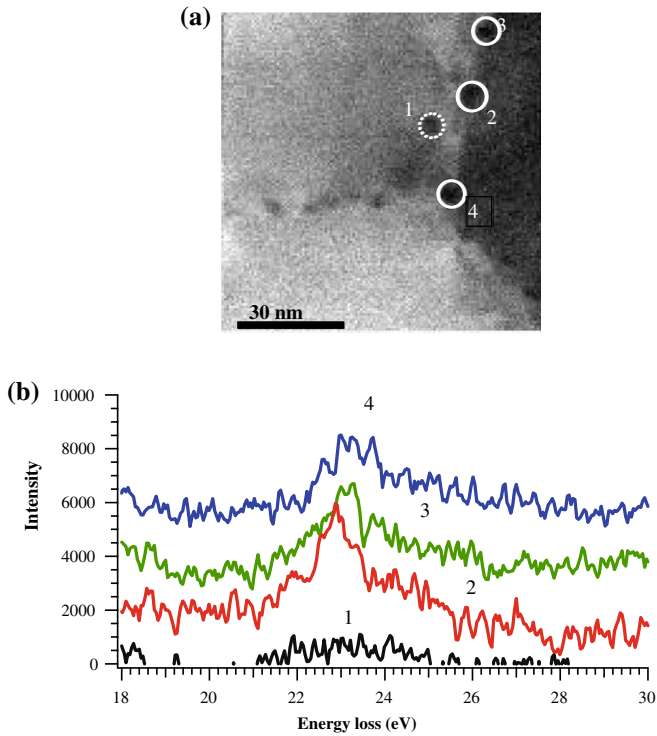
Fig. 4. (a) HAADF image of many He bubbles (with circles) and (b) subtracted spectra of these bubbles.

tion is that these voids have been produced during the thin foil preparation and have lost their He content.

4.2. Blue shift of the He 1s → 2p peak as a function of the bubble mean diameter

The He 1s → 2p energy position was measured on EEL spectra acquired for each analysed bubble and the energy shift was measured with respect to the free atom value of 21.218 eV [18]. In agreement with the literature results, an approximately linear relation between the measured energy shift (ΔE) and the average bubble inverse radii ($1/r$) is found (Fig. 5). The energy shift error attributed to each point is taken as the standard variation in the He peak energy position for the same pixel during the acquisition of a chronospim (acquisition of many spectra for each pixel) (±0.25 eV). The error on the bubble inverse radius is estimated by calculating the maximum and minimum inverse radii from the
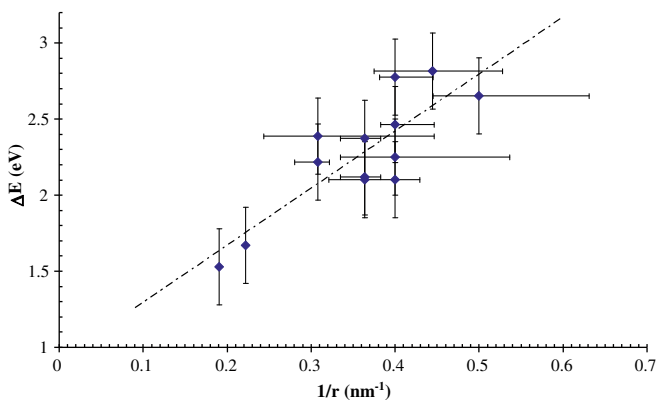
HAADF image for each not perfectly spherical bubble. The He density depends on the size of the bubble. Smaller bubbles correspond to higher He densities and thus to larger energy shifts. This "blue" shift is commonly attributed in the literature to the effect of the short-range Pauli repulsion, which comes from wave function overlap in neighbouring atoms. For bubbles of the same radius, the measured He peak energy position can be different. For example, for $r = 5$ nm, the energy shift ΔE can vary from 2.101 to 2.776 eV which could be explained by the fact that the bubble thickness may not be precisely estimated. The error in the measurement of the bubble diameter can be significant, especially when the bubbles are very small.

4.3. Estimation of the He density

The inelastic scattering cross-section used in the calculation of the He density was calculated using the Hartree-Slater model and depends on various experimental parameters, particularly the scattering angle. Under our experimental conditions, the values varied from 5.55×10^{-24} to 9.14×10^{-24} m² depending on spectrometer collection angle. The estimation of the He density was performed for all bubbles observed on the different studied areas and by the method explained in Section 3. Fig. 6 shows the evolution of the estimated He atom density as a function of the inverse bubble radii. The density error is calculated by applying standard error propagation relations to expression (2). A clear dependence of the He density on the inverse radii can be observed. The values of the estimated He density range from 20 to 70 nm⁻³. Compared to the density of liquid He (20 nm⁻³ at 2 K and for a pressure of 1 bar) [19], these values seem to be very high.

4.4. Pressure in He bubbles

The pressure inside the bubbles can be obtained from the values of the He density using an equation of state (EOS). As the estimated He densities are very high, the ideal gas law cannot be used. Among the various equations developed in the literature, that proposed by Trinkaus [2] corresponds best to our density range. The appropriate temperature to use in the equation is that at which the bubbles were formed, i.e. the implantation temperature. A linear relation between the pressure and the inverse radius can be clearly observed in Fig. 7. The slope of this curve is of the order 3 GPa nm (or J m⁻²). This is equivalent to an estimation of $\gamma = 1.5$ J m⁻², which is smaller than the value of the surface energy (2 J m⁻²) given for Fe in the literature [21]. At equilibrium, the pressure in the bubble is expected to be
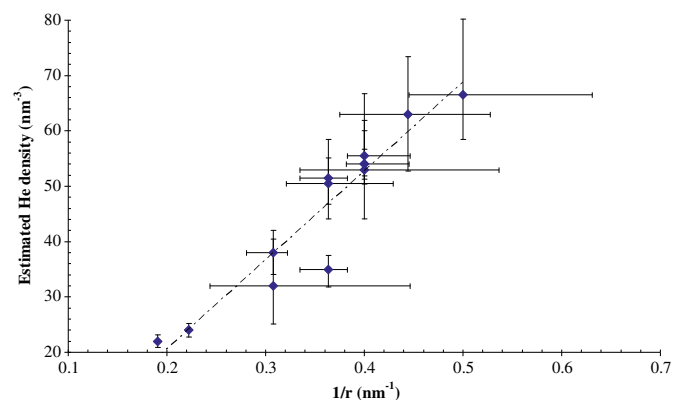
$$P \approx 2\gamma/r, \tag{3}$$

Fig. 5. Measured energy shift as a function of the inverse radii.

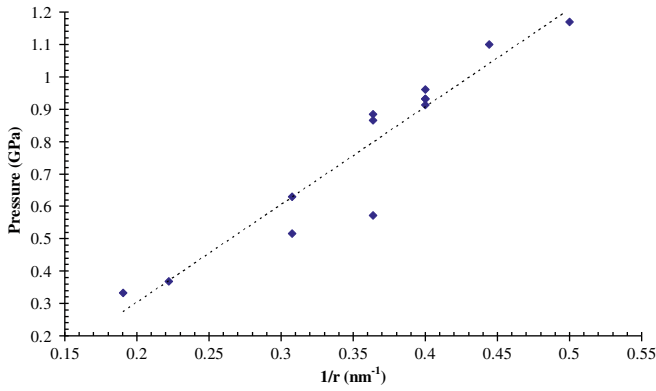**Fig. 6.** Estimated He density as a function of the inverse radii.

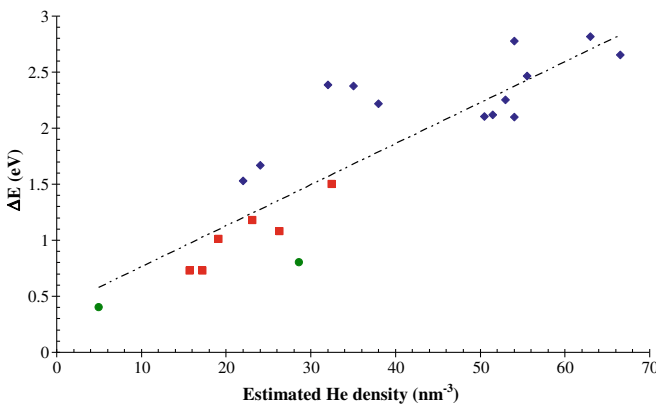**Fig. 7.** Relation between the pressure and the inverse radii.

Fig. 8. Measured energy shift as a function of the estimated He density for the results obtained in this work (blue) and those obtained by Walsh et al (green) and Taverna (red). (For interpretation of the references in colour in this figure legend, the reader is referred to the web version of this article.)

where γ is the surface energy. Thus despite the rather high helium density the pressure in the bubbles is still below what might be expected at equilibrium in the metal.

5. Discussion

In order to compare the results obtained in this work with those obtained elsewhere (with the same method for the estimation of the He density), a plot has been made of the energy shift versus He density for all results (Fig. 8). All data follow the same trend and can be fitted by a straight line: $\Delta E = Cn + \delta e = 0.036n + 0.39$. It is worth noting that a linear relation between ΔE and n is a good indication of the reliability of the measured He density.

Table 2 summarizes the values of C obtained both in this work and elsewhere. The value found here ($\Delta E = 0.019n + 1.36$) is close to those of Walsh and Jäger, but is considerably lower than those of Taverna and McGibbon. However, there is a good deal of scatter in the data, as is seen in Fig. 8. This is mostly

caused by the large error in the density due to the uncertainties in the bubble volumes. Also, it is worth noting that the law depends on the inverse on r so the smaller diameters of the bubbles studied here produce greater uncertainties in the volume estimates. The differences in the values of C are therefore not necessarily significant, especially in view of the small number of data points in the previously published work. For the data obtained by Lucas et al. [14] and Jäger et al. [15], the energy shifts were measured for many bubbles with different sizes. Furthermore, as pointed out by Walsh et al. [2], Jäger et al. [15] assumed the relationship between the pressure and the bubble radius in order to determine the He density in the bubbles. McGibbon et al. [20], Walsh et al. [2] and Taverna et al. [10] used the same technique as the one discussed in this paper in Section 3.

As mentioned in Section 4.4, the bubbles studied in this work were found to be under-pressured. The same result was found by Taverna [10] and Walsh [2] who also used the Trinkaus EOS. In the case of Walsh, the bubbles were produced in a PE16 alloy (44% Ni, 33% Fe, 17% Cr) by (n, α) reaction due to irradiation in a nuclear reactor at a temperature of about 550 °C. The bubbles studied by Taverna were formed by tritium β-decay in a $Pd_{90}Pt_{10}$ matrix at room temperature.

However, both authors measured lower helium densities. The value obtained for a bubble diameter of 5 nm in this work is $53 < n_{He} < 55.5 \text{ nm}^{-3}$ compared to 28.6 and 32.5 nm^{-3} obtained by respectively Walsh [2] and Taverna [10]. We do not consider this particularly surprising, given the very different conditions prevailing in our experiments. Indeed, the mechanism of bubble nucleation and growth is function in particular of the helium accumulation rate and total concentration, of the existence or not of correlated radiation damage and of the temperature range (in T/T_m, with T_m being the melting temperature) in the material under study (see for instance the review by Trinkaus and Singh [5]). A plausible explanation for this lower measured pressure could be that, once formed, the bubbles act as vacancy sinks.

Further elucidation of the details of the formation and growth processes will require reliable data obtained from the same material while varying the helium implantation conditions (in particular, the implantation temperature).

6. Conclusions

The aim of this paper was to analyse the He bubbles in an α-implanted EM10 steel and to determine precisely the density and pressure by EELS. The main results are the following:

- The SPIM technique has been successfully applied to this problem.
- The He density in individual bubbles has been quantified.
- The high quality data obtained allowed us to establish two linear relationships: one between the energy shift and the estimated He density, and another between the pressure and the inverse bubble radius.
- By applying the equation of state of Trinkaus, it has been shown that the bubbles are under-pressured, in the experimental conditions used here.

Table 2
Values of the proportionality coefficient between the He density and the energy shift ΔE, for different materials and implantation conditions, to be compared to the value obtained in this work with He-implanted EM10 steel grade (in eV nm^{-3}).

Authors [Ref.]	Lucas et al. [14]	Jäger et al. [15]	McGibbon et al. [20]	Walsh et al. [2]	Taverna [10]	This work
C_n (eV nm^{-3})	0.031	0.024	0.035	0.016	0.044	0.019
Matrix	Al	Al	PE16 alloy	PE16 alloy	$Pd_{90}Pt_{10}$	EM10

The further use of this local microscopy technique will help to improve the understanding of He bubble growth and evolution as function of the irradiation conditions.

Acknowledgement

References

[1] H. Trinkaus, Radiat. Eff. 78 (1983) 189.
[2] C.A. Walsh, J. Yuan, L.M. Brown, Philos. Mag. A 80 (2000) 1507.
[3] P. Jung, J. Henry, J. Chen, J.-C. Brachet, J. Nucl. Mater. 318 (2003) 241.
[4] J. Henry, P. Jung, J. Chen, J.-C. Brachet, J. Phys. IV 12 (2002) 103.
[5] H. Trinkaus, B.N. Singh, J. Nucl. Mater. 323 (2003) 229.
[6] C.H. Zhang, K.Q. Chen, Y.S. Wang, J.G. Sun, D.Y. Shen, J. Nucl. Mater. 245 (1997) 210.
[7] C.H. Zhang, K.Q. Chen, Z.Y. Zhu, Nucl. Instrum. and Meth. B 169 (2000) 64.
[8] J. Henry, M.-H. Mathon, P. Jung, J. Nucl. Mater. 318 (2003) 249.
[9] N. Yamamoto, T. Chuto, Y. Murase, J. Nagakawa, J. Nucl. Mater. 329–333 (2004) 993.
[10] D. Taverna, M. Kociak, O. Stéphan, A. Fabre, E. Finot, B. Décamps, C. Colliex, Phys. Rev. Lett. 100 (2008) 035301.
[11] H. Schroeder, H. Ullmaier, J. Nucl. Mater. 179–181 (1991) 118.
[12] A. Möslang, D. Preininger, J. Nucl. Mater. 155–157 (1988) 1064.
[13] J.C. Rife, S.E. Donnelly, A.A. Lucas, J.M. Gilles, J.J. Ritsko, Phys. Rev. Lett. 46 (1981) 1220.
[14] A.A. Lucas, J.P. Vigneron, S.E. Donnelly, J.C. Rife, Phys. Rev. B 28 (1983) 2485.
[15] W. Jäger, R. Manzke, H. Trinkaus, R. Zeller, J. Fink, G. Crecelius, Radiat. Eff. 78 (1983) 315.
[16] P.R. Taylor, Chem. Phys. Lett. 121 (1985) 205.
[17] Jaysen Nelayah, M. Kociak, O. Stéphan, F. Javier García de Abajo, M. Tencé, L. Henrard, D. Taverna, I. Pastoriza-Santos, L.M. Liz-Marzán, C. Colliex, Nature Phys. 3 (2007) 348.
[18] H.G. Kuhn, Atomic Spectra (1962) 132.
[19] C.M. Surko, G.J. Dick, F. Rief, W.C. Walker, Phys. Rev. Lett. 23 (1969) 842.
[20] A. McGibbon, Inst. Phys. Conf. Ser. 119 (1991) 109.
[21] A. Kelly, N.H. MacMillan, Strong Solids, 3rd Ed., Clarendon, 1986.